

Supplementary Materials for

Large-scale controls of propagation of the Madden-Julian Oscillation

Xianan Jiang*, Eric Maloney, and Hui Su

*Corresponding author. Email: xianan@ucla.edu

This PDF file includes:

Supplementary Figure 1. Propagation of the intraseasonal variability in ECHAM simulations.

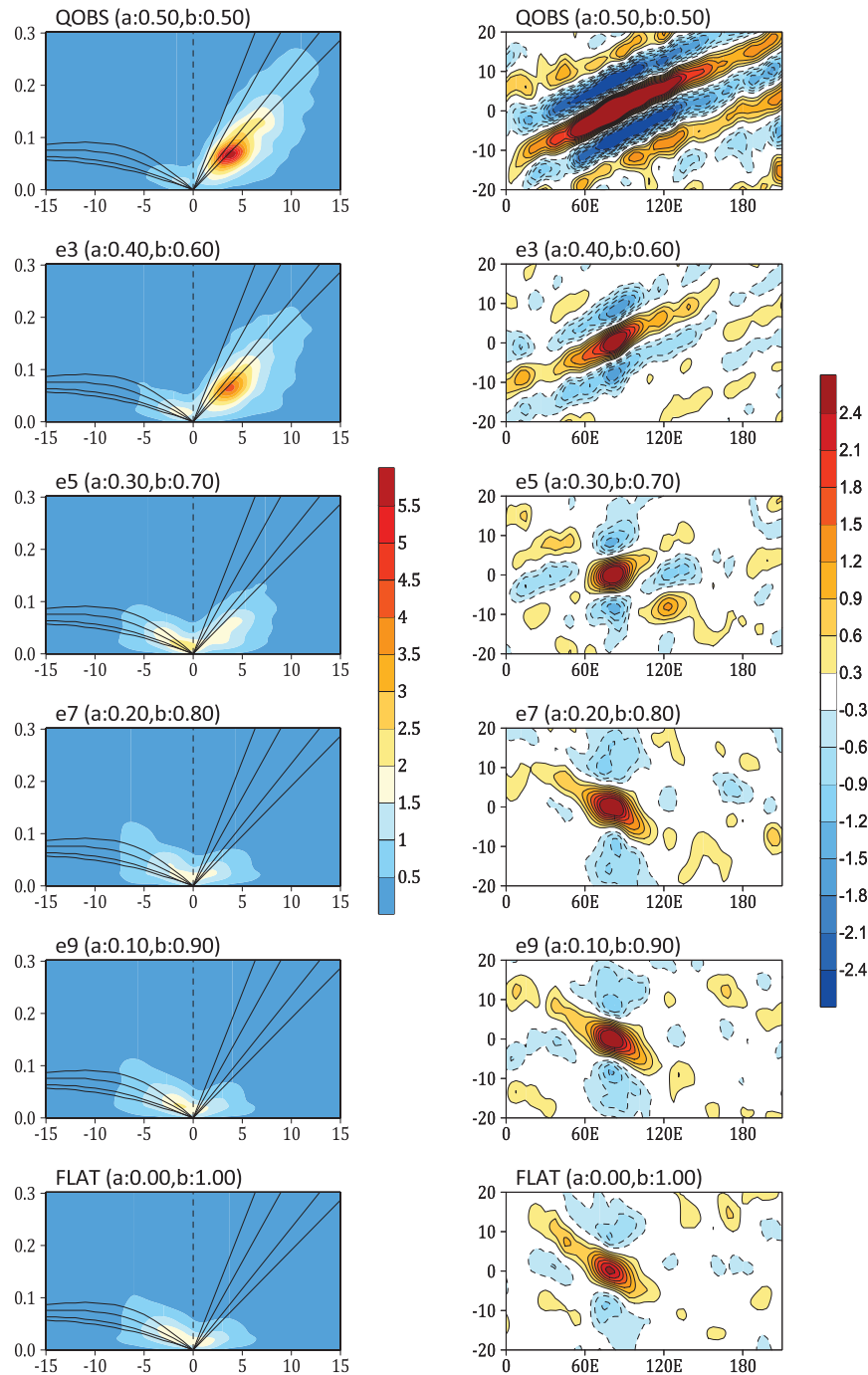
Supplementary Figure 2. Biases in winter mean lower-tropospheric moisture pattern in ECHAM simulations.

Supplementary Figure 3. Close association between convection and lower-tropospheric moisture perturbations associated with the intraseasonal variability.

Supplementary Figure 4. Moisture tendencies associated with the intraseasonal variability.

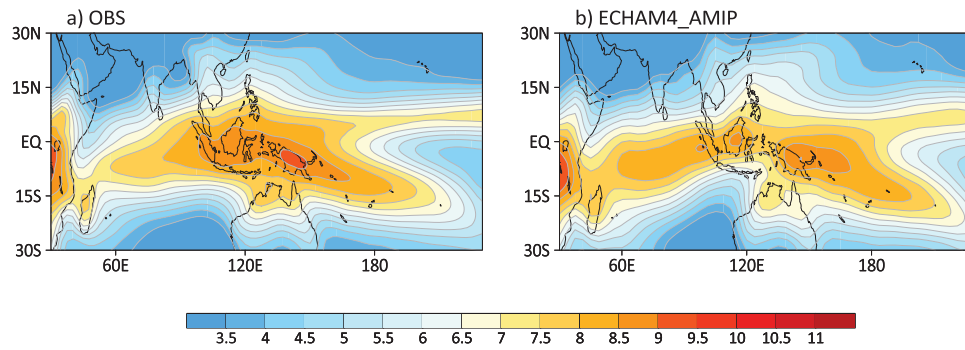
Supplementary Figure 5. Tendencies of vertically integrated moisture anomalies associated with the intraseasonal variability.

Supplementary Figure 6. Key processes responsible for total moisture tendency associated with the intraseasonal variability.

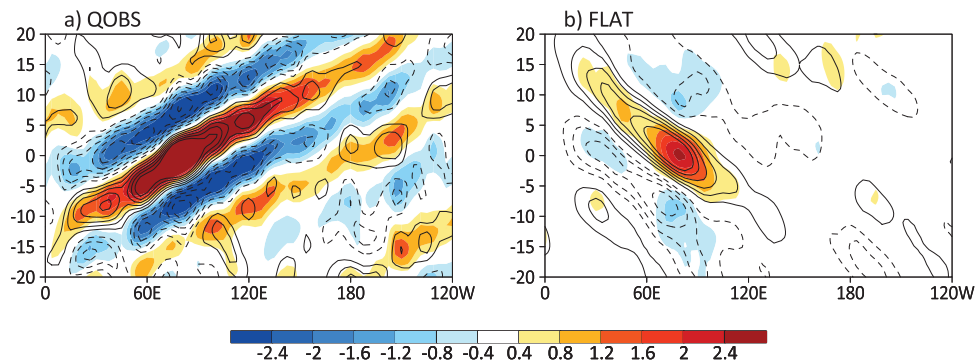


Supplementary Fig. 1 Propagation of the intraseasonal variability in ECHAM simulations. (Left)

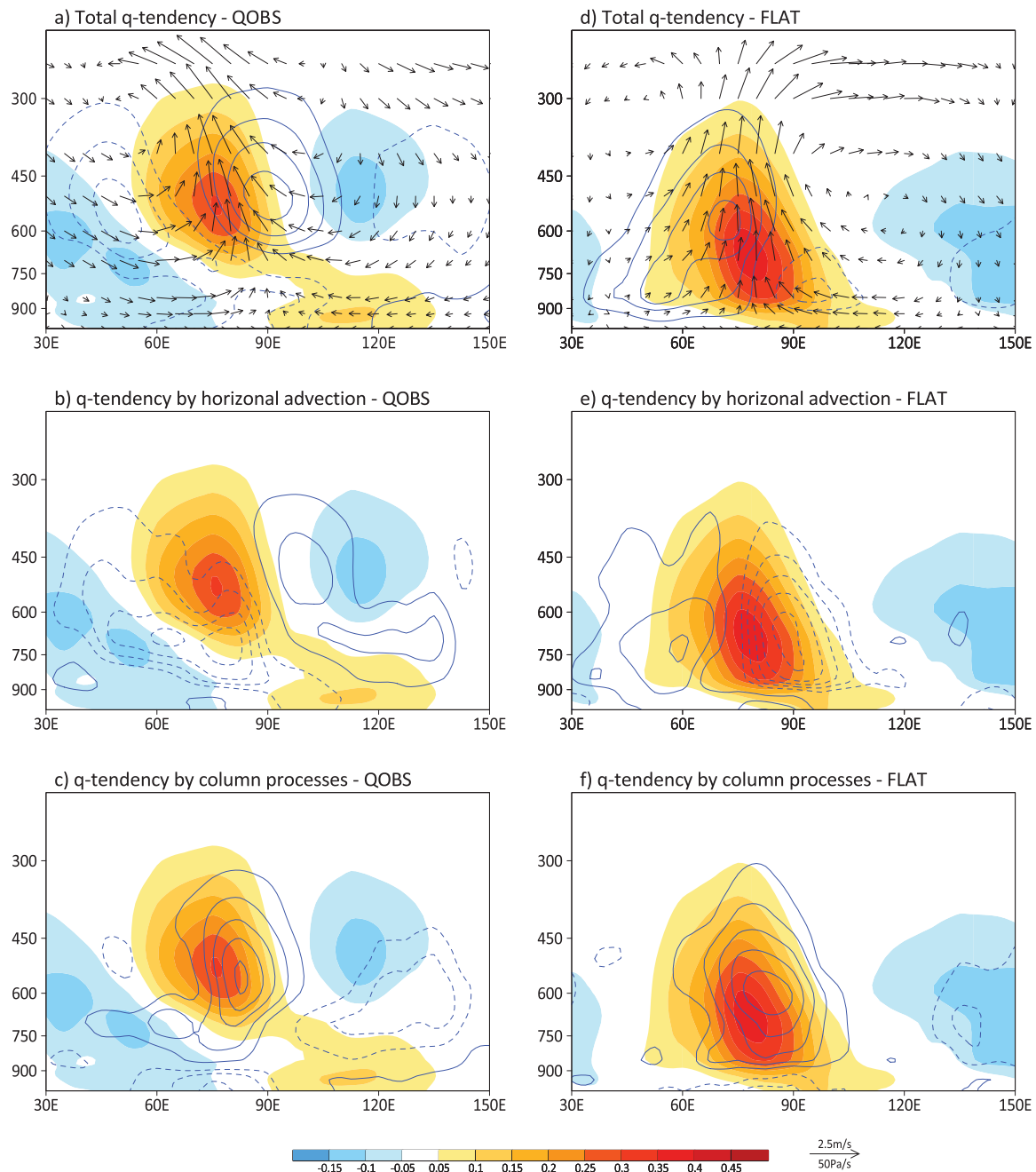
Spectral variances of symmetric rainfall anomalies (removal of climatological mean) about the equator on the wavenumber (x-axis) – frequency (y-axis) domain (15°S–15°N averaged). Superimposed are the dispersion curves of the equatorial waves for the four equivalent depths of 9, 12, 25, and 50m. (Right) Longitude-time evolution of rainfall anomalies along the equator (7.5°S–7.5°N averaged; units: mm day⁻¹) derived based on lag-regression of 10–90 day bandpass filtered anomalous rainfall against its averaged values over the Indian Ocean box (75–85°E; 5°S–5°N).



Supplementary Fig. 2 Biases in winter mean lower-tropospheric moisture pattern in ECHAM simulations. Winter (November-April) mean 850-400hPa averaged specific humidity in **a)** observations (ERA-Interim) and **b)** ECHAM AGCM forced by the observed climatological monthly mean SST (units: g kg⁻¹).

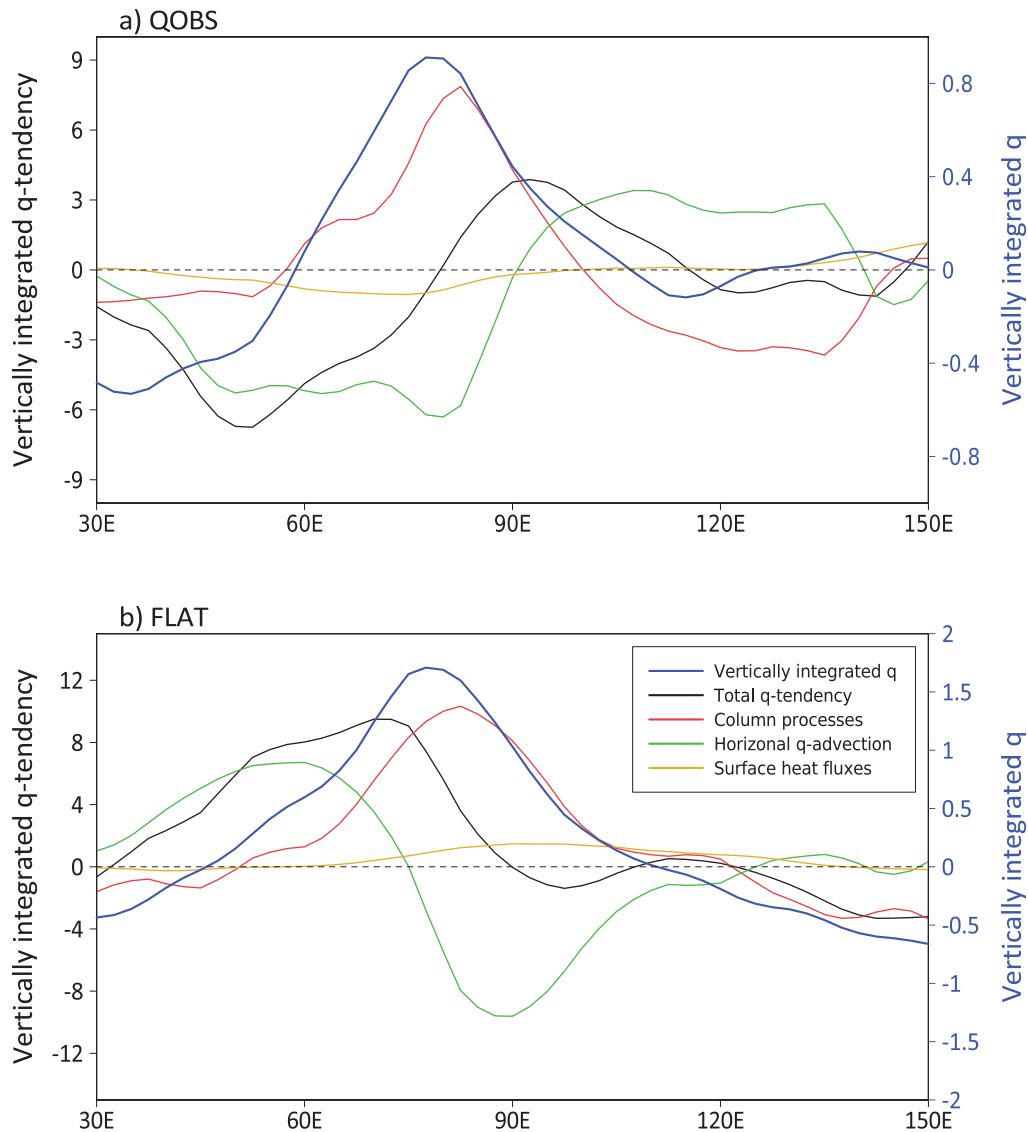


Supplementary Fig. 3 Close association between convection and lower-tropospheric moisture perturbations associated with the intraseasonal variability. (Shaded) Longitude-time evolution of rainfall anomalies along the equator (7.5°S - 7.5°N averaged; see color scale bar below; units: mm day^{-1}) in **a)** QOBS, and **b)** FLAT experiments as in Fig. 3c,d. (Contour) Similar as for rainfall, but for 850-400hPa averaged specific humidity perturbations (solid and dashed lines for positive and negative values respectively, with the first contour at 0.03 g kg^{-1} and an interval of 0.03 g kg^{-1}).

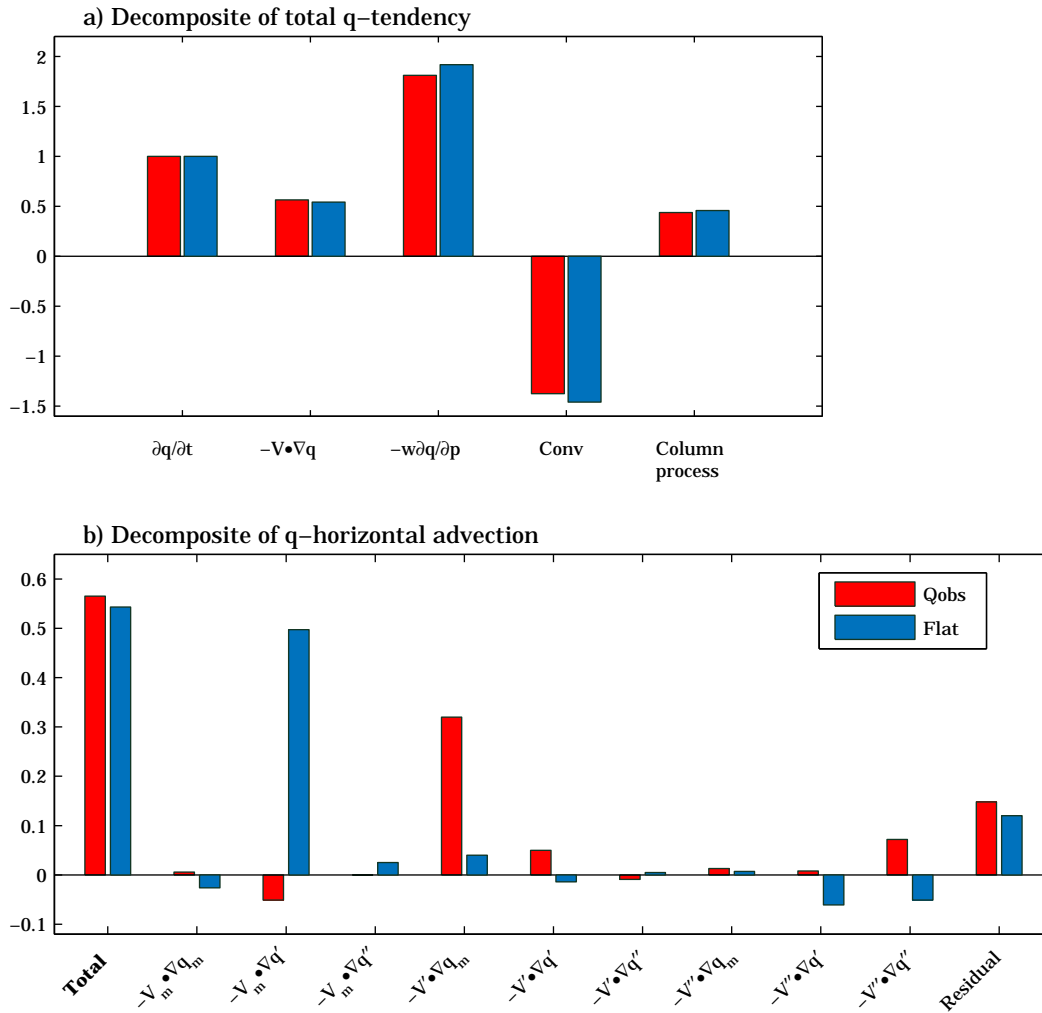


Supplementary Fig. 4 Moisture tendencies associated with the intraseasonal variability.

Longitude-pressure cross-sections of total moisture tendencies (top) and moisture tendencies due to horizontal advection (middle) and the column process (bottom) in contours along with moisture perturbations (shaded with color bar below the panel; unit: g kg^{-1}), and zonal versus vertical winds (vectors in top panels; see scale at the bottom) associated with the intraseasonal variability in QOBS (left) and FLAT (right). All perturbation fields are derived by lag0-regression of 10-90 day filtered fields against the intraseasonal rainfall index over the Indian Ocean as in Fig. 4, and are averaged over 7.5°S - 7.5°N . For contours of intraseasonal moisture tendencies in each panel, solid and dashed lines represent positive and negative values respectively, with the first contour at $1 \times 10^{-7} \text{ g kg}^{-1} \text{ s}^{-1}$ and an interval of $1 \times 10^{-7} \text{ g kg}^{-1} \text{ s}^{-1}$.



Supplementary Fig. 5 Tendencies of vertically integrated moisture anomalies associated with the intraseasonal variability. Vertically (1000-100hPa) integrated moisture anomalies (q ; unit: mm, right axis) and tendency terms (total, horizontal advection, and column process) along with surface heat flux anomalies (left axis; units: $W m^{-2}$) associated with the intraseasonal variability in a) QOBS and b) FLAT. All fields are derived by lag-0 regression of 10-90 day filtered fields against the intraseasonal rainfall index over the Indian Ocean as in Fig. 4, and are averaged over $7.5^{\circ}S$ - $7.5^{\circ}N$.



Supplementary Fig. 6 Key processes responsible for total moisture tendency associated with the intraseasonal variability. Relative role of **a)** each moisture tendency term and **b)** decomposition of horizontal advection by various time scales for the total moisture tendency associated with the intraseasonal variability based on QOBS (red) and FLAT (blue) experiments. In b), both horizontal winds and moisture fields are decomposed into three different time scales, i.e., low-frequency variability with a period greater than 90 days (denoted by the subscript “m”), intraseasonal time-scale with a period between 10 and 90 days (denoted by a prime), and high-frequency variability with a period shorter than 10 days (denoted by a double prime). See Methods for details.